RESEARCH ARTICLE

A record of the upper Olduvai geomagnetic polarity transition from a sediment core in southern Yokohama City, Pacific side of central Japan

Chie Kusu[1*], Makoto Okada[2], Atsushi Nozaki[3], Ryuichi Majima[4] and Hideki Wada[5]

Abstract

A detailed paleomagnetic record of the upper Olduvai polarity transition was obtained from a 106.72 m-long sediment core drilled in southern Yokohama City, located on the northern Miura Peninsula, on the Pacific side of central Japan. The core spans the upper part of the Nojima Formation and the lowermost part of the Ofuna Formation, both of which correspond to the middle Kazusa Group (Lower Pleistocene forearc basin fill). The record was reconstructed using discrete specimens taken throughout mudstone and/or sandy mudstone sequences in the Nojima Formation. In this record, the virtual geomagnetic pole (VGP) fluctuation accompanying the polarity transition was determined to occur between depths of 66.99 and 63.60 m. These depths have been dated at 1784.4 and 1779.9 ka, respectively, and the duration of the polarity transition is estimated to be 4.5 kyr using an age model based on a $\delta^{18}O$ record from that core. The VGP paths during the transition do not appear to show any preferred longitudinal bands. However, the VGP positions cluster in five areas: (A) eastern Asia near Japan, (B) the Middle East, (C) eastern North America (North Atlantic), (D) off southern Australasia, and (E) the southern South Atlantic off South Africa. The primary locations of the observed VGP clusters coincide with the areas on the Earth's surface that possess a strong downward flux of the vertical component of the present geomagnetic non-axial dipole field. The relative paleointensity rapidly decreased approximately 1 kyr before the beginning of the polarity transition and gradually recovered to its initial level in 12 kyr.

Keywords: Geomagnetism, Paleomagnetism, Geomagnetic polarity transition, Olduvai subchron, VGP path, VGP cluster, Reversal, Relative paleointensity, Sediment core

Introduction

Studies of geomagnetic reversals, which are among the most conspicuous phenomena associated with the Earth's magnetic field, provide valuable information about geodynamo processes. Previous paleomagnetic investigations have documented the details of geomagnetic field behavior during geomagnetic polarity transitions. The virtual geomagnetic poles (VGPs) during polarity transitions, as inferred from sediments, tend to pass within two preferred longitudinal bands over the Americas and antipodally over eastern Asia and through Australia (Tric et al. 1991; Clement 1991; Laj et al. 1991). Conversely, late Cenozoic volcanic records from intervals spanning polarity transitions suggest that VGPs were clustered mainly within two regions near the southern portions of South America and Western Australia (Hoffman 1991, 1992). These regions lie within the two preferred longitudinal bands identified in the sedimentary records. However, the VGPs inferred from the volcanic records appear not to have moved continuously but to have "jumped" between the regions. The two preferred bands coincide with the centers of the radial magnetic flux of the present geomagnetic field on the Earth's surface when the axial dipole component is removed (Hoffman 1992). Laj et al. (1991) reported that the two preferred

* Correspondence: kusu-chie-sf@ynu.jp
[1]Graduate School of Environment and Information Sciences, Yokohama National University, 79-7 Tokiwadai, Hodogaya-ku, Yokohama 240-8501, Japan
Full list of author information is available at the end of the article

Kusu *et al. Progress in Earth and Planetary Science* (2016) 3:26

Page 2 of 13

bands coincide well with regions of fast seismic wave propagation (regions of cooler temperature) observed in the lowest mantle. Therefore, they suggested that the transitional field was constrained by temperature patterns at the core-mantle boundary, and its configuration might have persisted over the past 10 Myr. Recently, several high-resolution sedimentary records from deep-sea cores have shown that transitional VGPs still passed within the preferred longitudinal bands but also stayed within regions similar to the VGP clusters observed in volcanic records (e.g., Mazaud and Channell 1999; Ohno et al. 2008; Mazaud et al. 2009).

The detailed processes relating to geomagnetic polarity reversals remain unclear, although it is generally accepted that field intensities during polarity transitions decline to ~10 % of their usual values, which is close to the magnitude of the non-dipole component of the current geomagnetic field (Merrill and McFadden 1999). Absolute paleomagnetic intensities are typically only recovered from the thermal remanent magnetization of volcanic rocks, but this does not yield a continuous record. Tauxe (1993) proposed a method to deduce relative paleointensities using sedimentary records, and continuous relative paleointensity records have thus been obtained from deep-sea sediments. In recent years, studies of relative paleointensity have progressed (e.g., Tauxe and Yamazaki 2007), and global stacks of relative paleointensity variations spanning the last 1 to 3 Myr have been generated (e.g., Valet et al. 2005; Yamazaki and Oda 2005; Channell et al. 2009). Those records, which have focused on reconstructing long-term variations in geomagnetic dipole moment, have been successful in revealing the broad features of geomagnetic dipole fluctuations. However, the details of paleointensity variations during polarity transitions are poorly documented because the accumulation rates of deep-sea sediments used to generate the stacked records are quite low (approximately a few cm/kyr). Because the average duration of polarity transitions has been estimated at 7 kyr, based on available sediment records spanning the four most recent transitions (Clement 2004), records with resolutions higher than 1 kyr are needed to observe detailed variations in paleointensity as well as direction during polarity transitions.

It is generally considered that the magnetization of sediments is stabilized through post-depositional remanent magnetization (PDRM) processes (Irving and Major 1964; Kent 1973). The fixing of magnetic particles in a sedimentary column is thought to occur gradually within a zone due to sediment compaction and dewatering, which generates an offset between the depth where the magnetization is fixed and the sediment surface (e.g., Verosub 1977; Hyodo 1984). This offset is referred to as the "lock-in depth" of PDRM and has been the focus of much debate for a long time (e.g., Okada and Niitsuma

1989; deMenocal et al. 1990; Tauxe et al. 1996, 2006; Channell and Guyodo 2004). Suganuma et al. (2010, 2011) convincingly showed that magnetization in a sedimentary column takes place within a zone just below the base of the bioturbation zone. Based on direct comparisons of ^{10}Be flux and paleomagnetic records through the Matuyama-Brunhes transition in deep-sea cores, they deduced by means of a Gaussian lock-in function that the thickness of the zone of magnetization is approximately 17 cm, regardless of the sedimentation rate. This indicates that sedimentary sequences with accumulation rates that exceed 17 cm/kyr are enough to reconstruct records of past geomagnetic field fluctuations with a time resolution of 1 kyr. Although the PDRM process is uncertain and still under debate, it is possible to minimize the length of delay and smoothing width in remanence acquisition due to the PDRM process by using a sediment sequence that has as high a sedimentation rate as possible.

In this paper, we present an ultra-high-resolution paleomagnetic record of the upper Olduvai polarity transition from a sediment core comprising a homogeneous siltstone whose sedimentation rate exceeded 70 cm/kyr. We also present the VGP paths and relative paleointensity variations during the transition.

Methods/Experimental
Geology of the core site
The core used in this study (Core M; 35.354 6° N, 139.606 3° E) was recovered from the middle part of the lower Pleistocene Kazusa Group in September 2010 using a rotary drilling method and an 86 mm diameter bit. The core is 106.72 m long and composed of sediments with almost 100 % recovery (Fig. 1). The Kazusa Group, a forearc basin fill, is exposed in the northern Miura Peninsula, central Japan. Core M is composed of the upper part of the Nojima Formation (alternations of mudstones and sandy mudstones below a core depth of 20.5 m) and overlies the lowermost part of the Ofuna Formation (massive mudstones from the top of the core to 20.5 m) in the middle part of the Kazusa Group.

The depths at which the sediments of the Nojima and Ofuna Formations were deposited are estimated to 400 to 500 m in the lower horizon of the Nojima Formation (Utsunomiya and Majima 2012) and 200 to 300 m in the upper horizon of the Ofuna Formation (Tate and Majima 1998; Kitazaki and Majima 2003). The strike and dip of the bedding around the Core M site are N63° W and 12° NE, respectively, based on outcrop observations of the NOT-1 tuff bed (Nozaki et al. 2014; the YH02 tuff bed of Takahashi et al. 2005 and Kusu et al. 2014), which is intercalated with sediments between 14.46 and 14.41 m depth in Core M. The detailed lithologies of Core M will be described in a separate paper.

Kusu *et al. Progress in Earth and Planetary Science* (2016) 3:26

Page 3 of 13

In May 2004, Core I (105.00 m in total length; 35.357 5° N, 139.589 5° E) was drilled and recovered approximately 1.6 km west of the Core M drill site (Fig. 1c), and Kusu et al. (2014) published a paleomagnetic study of the upper Olduvai polarity transition and the vicinity in this core. In Core I, the upper Olduvai polarity transition was determined to lie between 86.77 and 84.64 m depth in the Nojima Formation on the basis of paleomagnetic inclination data at a horizon below the NOT-1 tuff bed that is intercalated between 27.03 and 26.83 m core depth. Core I was shown to provide a detailed record of the paleomagnetic behavior during the upper Olduvai transition; however, the record consists only of *in situ* paleomagnetic inclinations. Because Core I was stored as horizontally unoriented pieces of sections, information on the core's orientation and thus the declinations were lost. Conversely, when the newly recovered Core M was drilled, its orientation was recorded and described, thus enabling the reconstruction of the paleomagnetic vectors through the upper Olduvai polarity transition.

Paleomagnetic and rock-magnetic measurements

Core M was not initially oriented in a horizontal plane. Thus, the absolute declination values could not be directly obtained; however, the relative declination has been preserved within a continuously recovered interval without any core break. Because the core barrel used for the drilling was 2 m long, a 2 m-long continuous core segment was recovered at each stroke in the drilling operation. To determine the relative declinations for as long a continuous interval as possible, for each core segment, we confirmed whether its end surface could be connected to the next core segment and carefully checked the connection between the two segments without any horizontal rotation to ensure the continuity of the core. Additionally, when the dip of a bedding plane was identified from the sedimentary structures in the core, we drew a vertical orientation line at the position of the maximum dip direction on the core surface. Even when the dip could not be identified, we drew a vertical line on the core surface to ensure the directional continuity of the core segments.

For paleomagnetic and rock-magnetic measurements, 25.4 mm diameter mini-cores were collected horizontally from the side surface of the core along the vertical line marked on the core surface. The mini-cores were taken using a core-picker every 1 m over the entire core interval, every 10 cm between 85.00 and 75.20 m and
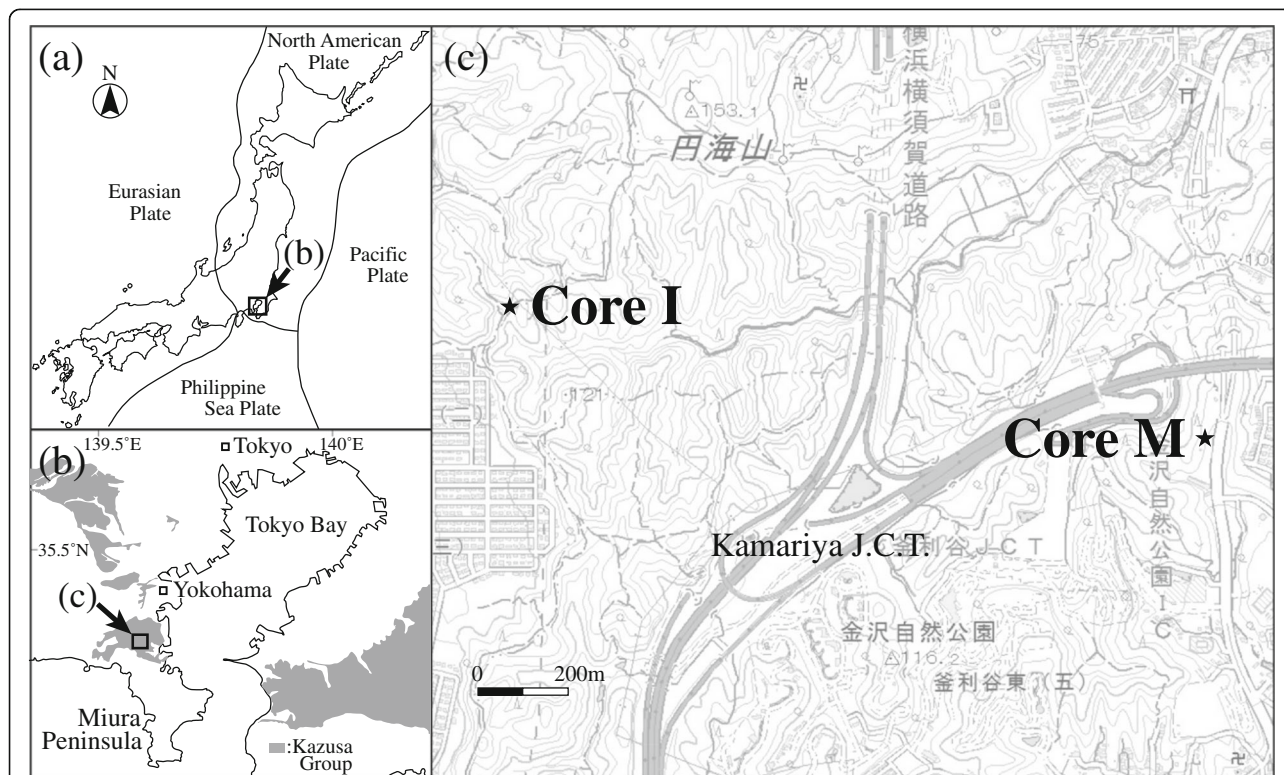

Fig. 1 Location maps of the study site. **a** Tectonic plates under the Japanese Islands (modified from Fig. 1 of Seno and Takano 1989). **b** Distribution of the Kazusa Group in the southern Kanto region (compiled from Mitsunashi and Suda 1980; Mitsunashi et al. 1980; Unozawa et al. 1983; Eto 1986; and Sakamoto et al. 1987). **c** Locality map showing the core sites (*solid stars*) plotted on a 1:25,000 scale topographic map published by the Geospatial Information Authority of Japan

Kusu *et al. Progress in Earth and Planetary Science* (2016) 3:26

Page 4 of 13

between 60.00 and 50.00 m and every 5 cm between 75.20 and 69.84 m. Each mini-core was cut into approximately 2 cm-long sections. Between depths of 69.84 and 60.00 m, the core was quartered vertically using a rock cutter, and one quarter of the core was cut continuously into approximately 2 cm-long cubic blocks from the center portion of the core. In total, specimens were obtained from 766 horizons in Core M.

Before demagnetization experiments were carried out, low-field magnetic susceptibility (volumetric) and anisotropy of magnetic susceptibility (AMS) measurements were performed on all specimens using a KLY-3 Kappabridge susceptibility meter (AGICO, Czech Republic). The natural remanent magnetization (NRM) was measured using an RF-SQUID Cryogenic magnetometer model 750R (2G Enterprises, USA). Progressive alternating field demagnetization (AFD) with a static 3-axis was performed in 5 mT increments up to 60 mT using a separate AF demagnetizer (DEM-8601C, Natsuhara-Giken, Japan), and progressive thermal demagnetization (THD) was performed in 50 °C increments up to 600 °C in air using a thermal demagnetizer (TD-48, ASC Scientific, USA). The measurements were performed at Ibaraki University, Japan. To deduce relative paleointensity, progressive AFD must be employed as the main demagnetization technique because after the demagnetization of the NRMs, the same specimen is repeatedly used for the acquisition of artificial remanent magnetizations to estimate relative paleointensities. The results of the progressive AFD and THD were displayed using an orthogonal vector diagram (Zijderveld 1967). Characteristic remanent magnetization (ChRM) directions were determined by principal component analysis (Kirschvink 1980) using more than five vector endpoints.

Relative paleointensity was estimated by normalizing for the magnetic grain content using anhysteretic remanent magnetization (ARM). Subsequent to the AFD of the NRM, the ARM was imparted to each specimen using a 30 μT DC field in an alternating field that decreased from a peak of 60 mT. After the ARM acquisition, AFD was then performed at 20, 30, 40, 50, and 60 mT to calculate the paleointensity proxy (NRM/ARM). Thermomagnetic analyses were performed on two samples (from depths of 70.01 and 58.58 m, near the polarity transition) using a Curie Balance NMB-89 (Natsuhara-Giken, Japan). The samples were heated to 700 °C and cooled in air and in a vacuum with an applied field of 0.3 T. Magnetic hysteresis was measured on eight samples at 2–3 m intervals between 70 and 50 m in Core M using a MicroMag 2900 alternating-force gradient magnetometer (Princeton Measurements, USA) to peak fields of ±1 T. The thermomagnetic experiments and hysteresis measurements were performed at the Kochi Core Center, Japan.
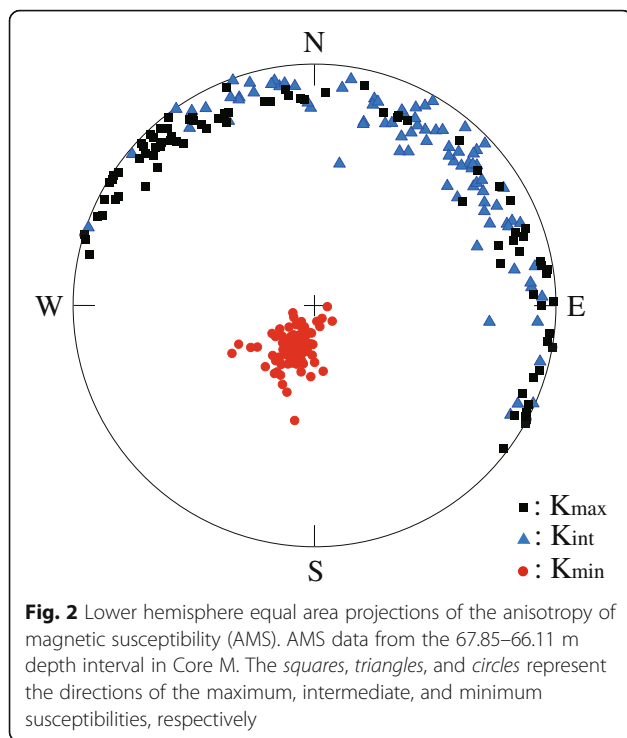
Oxygen isotope measurements

Stable oxygen and carbon isotopic ratios were measured to establish an age model based on correlation with the LR04 curve, which is a stacked $\delta^{18}O$ curve that uses oxygen isotope ratios measured in benthic foraminifers from 57 globally distributed deep-sea cores (Lisiecki and Raymo 2005). The isotopic measurements were performed on tests of the planktonic foraminifer *Globorotalia inflata*. Because *G. inflata* precipitates its test at approximately 300–500 m below the sea surface where water temperatures are relatively constant, the *G. inflata* $\delta^{18}O$ profile tends to be parallel to that of benthic foraminifers (Oba et al. 2006). To extract the *G. inflata* tests, a total of 104 sediment samples were collected from the core at approximately 1 m intervals. Each dried sediment sample (approximately 80 g) was crushed and disaggregated using a sodium sulfate solution. From each sediment sample, we picked tests of *G. inflata* that were unbroken, untarnished, "glassy," and larger than 250 μm in size. Each test was immersed in ethanol, broken using a needle, and then ultrasonically cleaned to remove filling impurities.

The isotopic measurements were performed at Shizuoka University, Japan, using the procedure of Wada et al. (1984). The 20–30 individual tests used for each measurement were reacted in saturated phosphoric acid at 60 °C, and the evolved CO_2 gas was analyzed with a MAT-250 mass spectrometer. The obtained value was converted into a value against a PDB standard employing the US National Bureau of Standards NBS-20 (Vienna PDB). The standard deviations of the in-house standard (total of 19 measurements) were 0.04 ‰ for $\delta^{18}O$ and 0.02 ‰ for $\delta^{13}C$, which represented the precisions of the isotopic measurements.

Results
Rock magnetism

The magnetic fabrics were analyzed via AMS. The directions of the maximum susceptibility (K_{max}), intermediate susceptibility (K_{int}), and minimum susceptibility axes (K_{min}) of the AMS ellipsoids were plotted on lower hemisphere equal area projections. Figure 2 shows the AMS data for depths of 67.85–66.11 m within the same core segment for which the directional continuity was confirmed. The data are not corrected for tilt. The directions of K_{max} and K_{int} indicate a girdle distribution perpendicular to K_{min}, which indicates a flattening fabric, and all results of the AMS analysis showed similar flattening fabrics (foliations). The mean inclination of K_{min} between depths of 67.85 and 66.11 m was 74°, and the dip of the foliation plane formed by K_{max} and K_{int} is therefore estimated to be 16°. The estimated dip angle of the bedding plane at the core site is approximately 12°, which suggests that the foliation plane reasonably

Kusu *et al. Progress in Earth and Planetary Science* (2016) 3:26

Page 5 of 13

Fig. 2 Lower hemisphere equal area projections of the anisotropy of magnetic susceptibility (AMS). AMS data from the 67.85–66.11 m depth interval in Core M. The *squares*, *triangles*, and *circles* represent the directions of the maximum, intermediate, and minimum susceptibilities, respectively

coincides with the bedding plane. In the four sections of the core, bedding planes comprised of intercalated thin sandstone beds were directly examined. In each segment, the difference between the observed maximum

dip direction and the direction of the foliation plane was less than 10°. Accordingly, we treat the foliation plane, as deduced from the AMS data, as a bedding plane at the site.

Thermomagnetic curves from samples at depths of 70.01 and 58.58 m are shown in Fig. 3. Both curves show an identical Curie temperature of approximately 570 °C, which indicates that magnetite (or Ti-poor titanomagnetite) is the predominant magnetic carrier. The heating curves in air as well as in vacuum show a slight increase above 450 °C, but the cooling curves do not show such inflections. When iron sulfide minerals such as pyrite are present in sediments, they are changed into magnetite and maghemite and, finally, into hematite through heating by oxidation that occurs primarily above 450 °C, which produces a heating curve that at first shows an increase in the magnetization and then a decrease (Passier et al. 2001). Therefore, although the thermomagnetic curves suggest a minor amount of iron sulfide minerals, (titano)magnetite is considered to be the main magnetic mineral in the samples.

A plot of anhysteretic remanent magnetization susceptibility (κ_{ARM}) versus magnetic susceptibility (κ) for Core M and Core I is shown in Fig. 4a. According to the grain size estimates of King et al. (1983), the mean grain sizes of the magnetic grains in the specimens from Core M and Core I should primarily range from 1 to 5 μm. Figure 4b shows a Day plot (Day et al. 1977) using
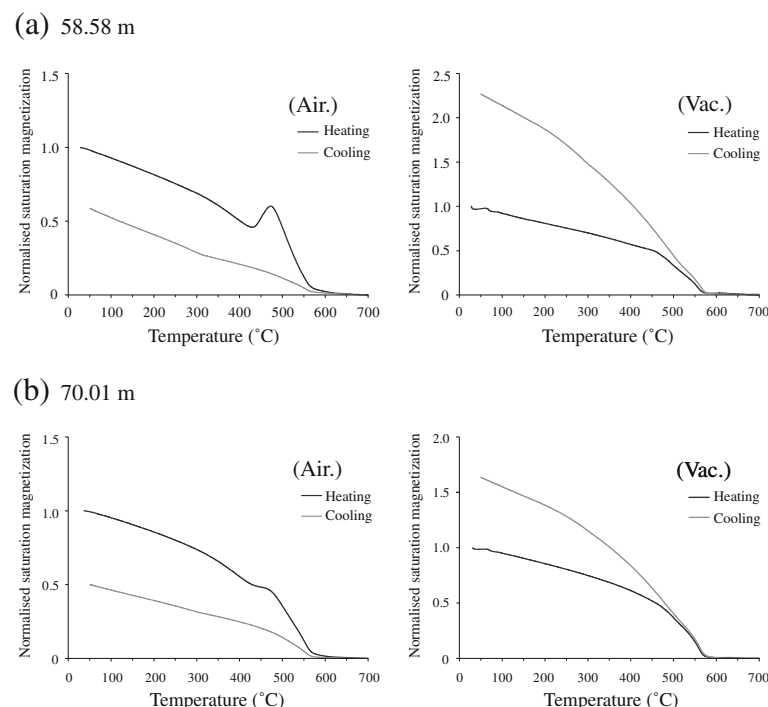

Fig. 3 Strong-field thermomagnetic behaviors. **a** sample from the depth of 58.58 m, **b** sample from the depth of 70.01 m in Core M. Air.: Under an air condition. Vac.: Under a vacuum condition

Kusu *et al. Progress in Earth and Planetary Science* (2016) 3:26

Page 6 of 13

selected specimens from Core M and Core I. Both plots indicate that pseudo-single domain (PSD) or mixture of single domain (SD) and multidomain (MD) magnetite grains are the predominant magnetic carriers. The Core I data are from Kusu et al. (2014).

A plot of the magnetic susceptibility (κ) and anhysteretic remanent magnetization susceptibility (κ$_{ARM}$) on a logarithmic horizontal scale is shown in Fig. 6g. The κ and κ$_{ARM}$ show similar gradual fluctuations, which range within an order of magnitude. Additionally, the fluctuation patterns of κ and κ$_{ARM}$ strongly resemble each other. Therefore, it is possible that the changes in the values of κ and κ$_{ARM}$ are related to changes in the magnetic mineral content in the specimen, and the changes in the magnetic mineral content with depth are relatively small.

Remanent magnetization

Typical orthogonal vector diagrams for NRMs during progressive AFD and THD are shown in Fig. 5. Most of the results show that the secondary magnetization components were removed by AF demagnetization at a peak field strength of 15 mT. Large fluctuations in the inclinations can be recognized between depths of 67.03 and 64.38 m (Fig. 5e), and steep upward inclinations are observed between depths of 64.36 and 63.20 m (Fig. 5d). In the lower part, below a depth of 67.05 m, the inclinations are positive (Fig. 5b, f), and the maximum angular dispersion (MAD) values for the ChRMs are generally less than 5°. However, values slightly over 10° are seen in a few specimens just below a depth of 67.05 m (Fig. 6d). In the upper part, above a depth of 63.18 m, the inclinations are negative (Figs. 5a, c), and the MAD values for the ChRMs are generally less than 10°, approximately 80 % of which are less than 5° (Fig. 6d). ChRMs were not obtained from five specimens (from depths of 66.61, 66.59, 66.55, 66.49, and

65.81 m), which had very weak remanences (Fig. 5g) and/or MAD values exceeding 25°. From these inclinations, we infer that the Olduvai normal polarity subchronozone occupies the lower part below a depth of 67.05 m, and the post-Olduvai Matuyama reversed polarity chronozone occupies the upper part above a depth of 63.18 m.

Orientation of the core

The core was not oriented, and absolute paleomagnetic declinations therefore could not be derived directly from the measured ChRMs. To obtain the declinations of the ChRMs, we reconstructed the core orientation via the following process. First, we calculated the dip azimuth of the foliation plane, which was deduced from the AMS in each core segment where the continuity of the cores was confirmed. We then adjusted the dip azimuth to the north direction. Using this process, we connected core segments between depths of 80 and 50 m. However, significantly different declinations of ChRMs were observed at three depth intervals: 79.78 to 76.59 m, 73.71 to 72.05 m, and 51.48 to 51.17 m (intervals are indicated by the gray bars in Fig. 6b). We then readjusted the azimuth directions at the three intervals to minimize the differences in the declinations between the three intervals and other depths. Next, the dip azimuth observed in the core was adjusted to the dip azimuth of the bedding plane observed around the core site (strike and dip: N63° W and 12° NE), and the tilt was then corrected. Finally, the mean declination of the normal polarity (below 67.05 m) was adjusted to 0°.

Paleomagnetic directional changes and relative paleointensity

The resultant declinations and inclinations of the ChRMs are shown in Fig. 6a, c. The reversed polarity declinations were generally aligned to 180°, and the
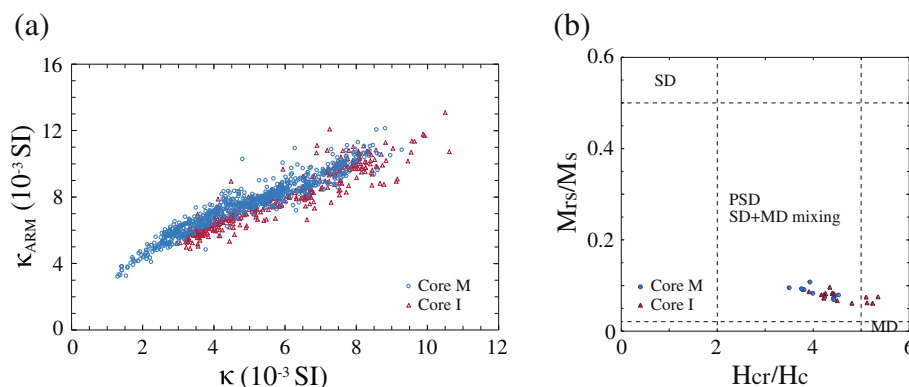

Fig. 4 Rock-magnetic results. **a** Anhysteretic remanent magnetization susceptibility (κ$_{ARM}$) plotted against volume magnetic susceptibility (κ). **b** The Day plot used selected specimens from Core M and Core I (Day et al. 1977). *Mrs* saturation remanent magnetization, *Ms* saturation magnetization, *Hcr* remanent coercivity, *Hc* coercivity. *SD*, *PSD* and *MD* indicate single domain, pseudo-single domain, and multidomain fields, respectively, with the limits given by Dunlop (2002)

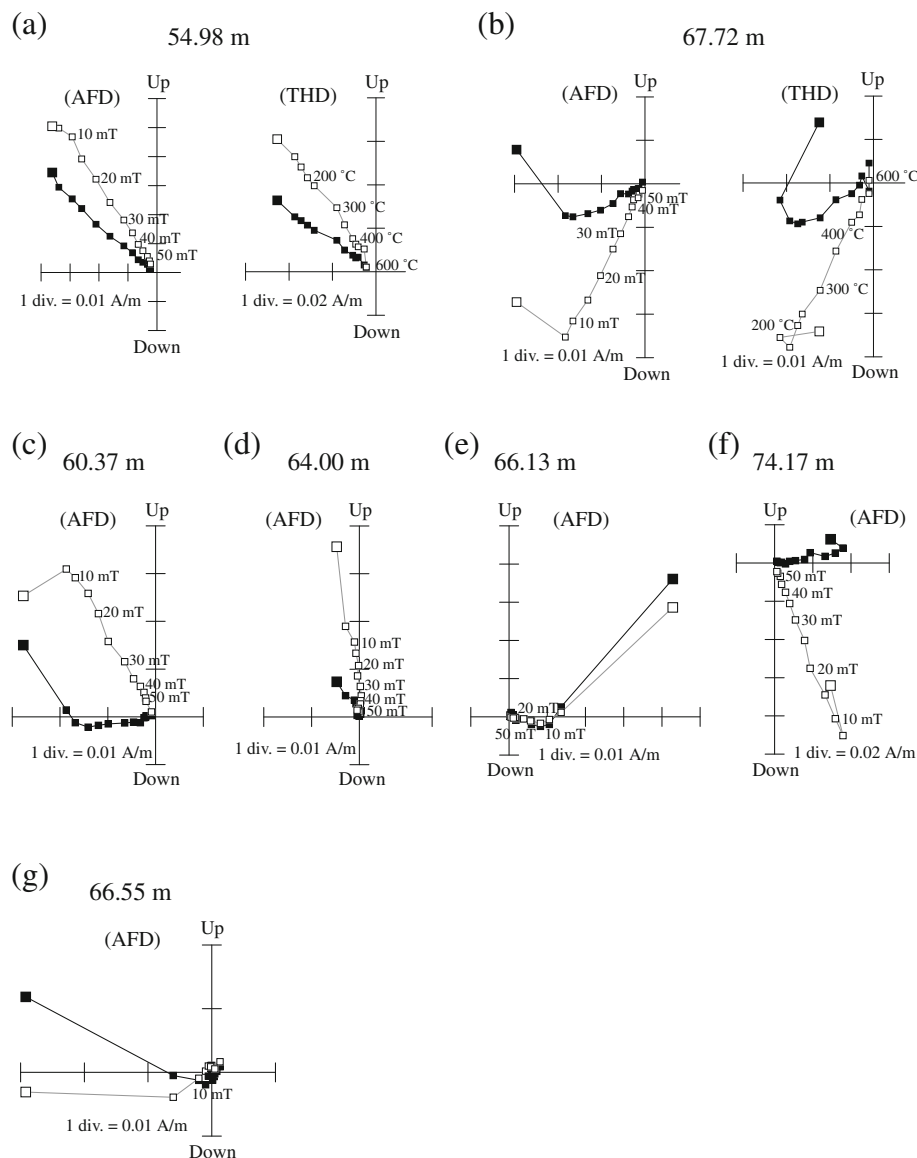Kusu *et al. Progress in Earth and Planetary Science* (2016) 3:26

Page 7 of 13

Fig. 5 Examples of demagnetization diagrams. Typical results from the orthogonal vector diagrams for data obtained during progressive thermal demagnetizations (*THD*) and alternating-field demagnetizations (*AFD*) for samples from Core M. **a**, **c** Samples from the post-reversal zone. **d**, **e** Samples from the transitional zone. **b**, **f** Samples from the pre-reversal zone. **g** Sample from a section yielding weak remanence intensity. The *solid* and *open symbols* indicate the projection of the vector endpoints onto the horizontal and vertical planes, respectively

inclinations after the tilting correction were aligned to ±53°, which would be expected given a geocentric axial dipole (GAD) at the core site. Large fluctuations in the declinations and inclinations were observed between depths of 67.03 and 64.38 m, and steep upward inclinations were observed at approximately 63.5 m depth. The VGP latitudes calculated from the ChRMs are shown in Fig. 6e. The VGP moves across the equator from the Northern Hemisphere to the Southern Hemisphere between 65.69 and 65.67 m depth. The VGP begins to move rapidly at a depth of 67.03 m, and the VGP settles at approximately 63.44 m after moving to the Southern Hemisphere.

The rock-magnetic measurement results indicate that the predominant carrier of magnetic remanences in the sediments is PSD, or a mixture of SD and MD-sized (titano)magnetite (Figs. 3 and 4), and the fluctuations in κ and κ_{ARM} range within an order of magnitude (Fig. 6g). From these results, the sediment satisfies the criteria for relative paleointensity reconstruction proposed by Tauxe (1993). To obtain an appropriate proxy for relative paleointensity, we compared the NRM/ARM ratios from three different coercivity fractions, which were between 20 and 40 mT, 30 and 50 mT, and 30 and 40 mT. The variations of the three coercivity fractions were almost
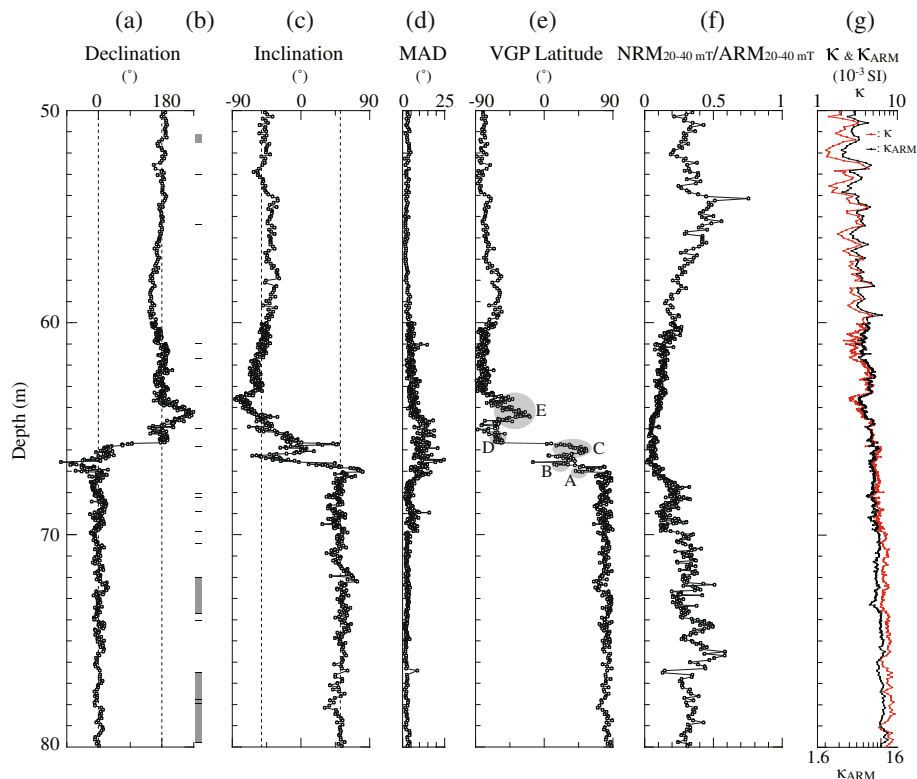
Fig. 6 Rock-magnetic and paleomagnetic results from a depth interval of 80–50 m in Core M. **a** Paleomagnetic declinations. **b** Section breaks. **c** Paleomagnetic inclinations. **d** Maximum angular dispersions (*MAD*) of principal component analysis. **e** VGP latitudes, in which the letters *A–E* are the VGP cluster locations see in Fig. 7a. **f** Relative paleointensities (NRM$_{20-40\ mT}$/ARM$_{20-40\ mT}$). **g** Volume magnetic susceptibilities (κ) and anhysteretic remanent magnetization susceptibilities (κ$_{ARM}$). The *vertical dotted lines* are the expected declinations and inclinations for the two polarities at the core site from the geocentric axial dipole field

identical, and we therefore used the NRM/ARM ratio between 20 and 40 mT as a proxy for relative paleointensity in this study (Fig. 6f).
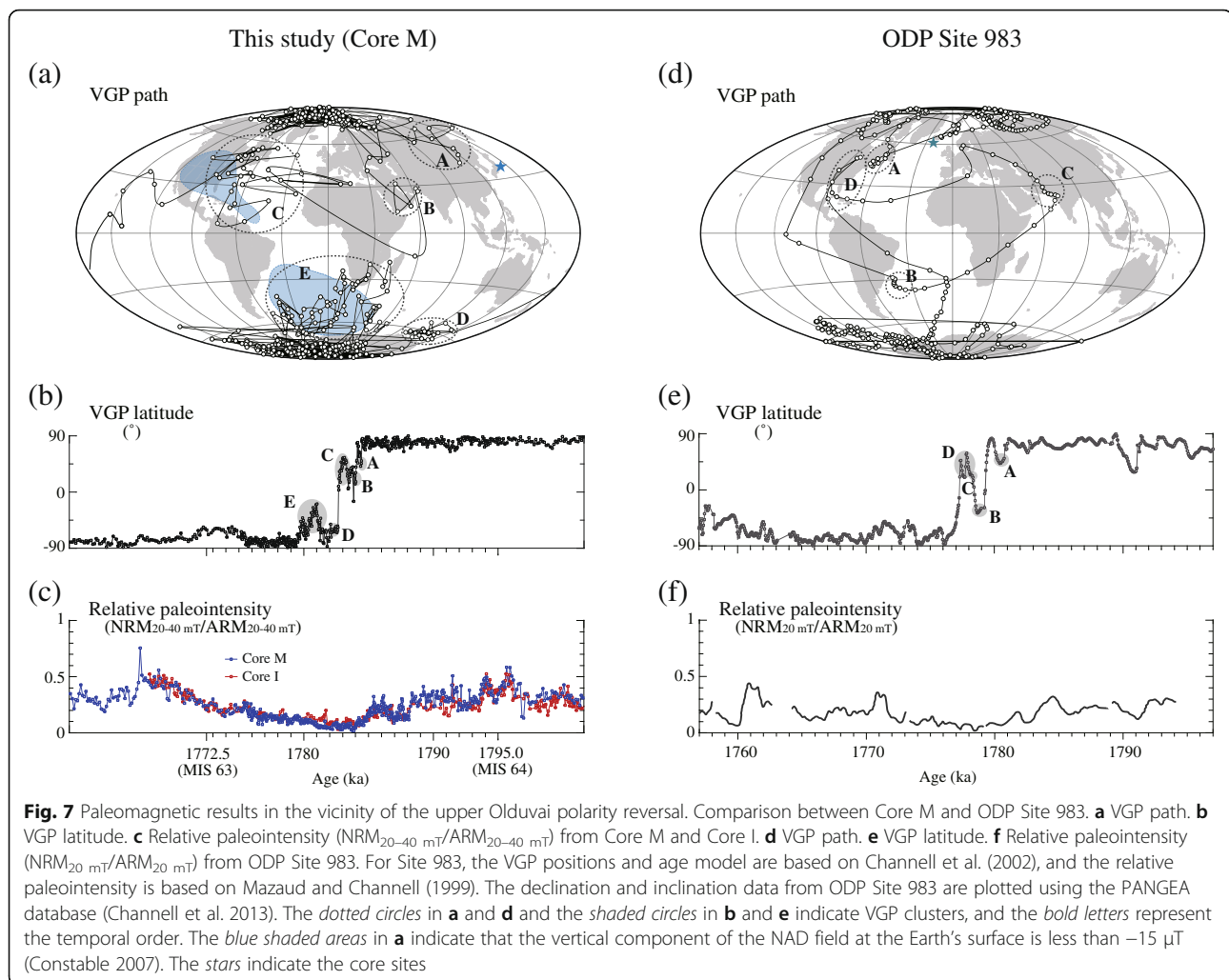
VGP and paleointensity
The VGP paths between 70.0 and 60.0 m are shown in Fig. 7a. In the upper Olduvai polarity transition, the VGP apparently did not move within a preferred longitudinal band but settled in several VGP cluster areas. The VGP can be observed in five areas (Fig. 7a): (A) eastern Asia near Japan, (B) the Middle East, (C) eastern North America (North Atlantic), (D) off southern Australasia, and (E) the southern South Atlantic off South Africa. The VGP apparently moved rapidly between the clusters.

In the relative paleointensity of the normal polarity, a maximum value is observed at 75.50 m depth (Fig. 6f) and it then decreases with the short-term oscillations. Before the onset of the paleomagnetic directional change, the relative paleointensity has a peak at 67.75 m depth (with a value approximately 56 % of the maximum value), and values then decrease at 67.15 m to approximately 11 % of the maximum value. Subsequently, the

relative paleointensity slightly recovers up to 66.89 m. In this interval, the directional change begins at a depth of 67.03 m, and the VGP near the North Pole rapidly moves to cluster A (Fig. 6e). The relative paleointensity subsequently drops at 66.5 m depth. Between 66.53 and 65.81 m, the relative paleointensity is approximately 9 % of the maximum value. In the same interval, the VGP settles in cluster C. The relative paleointensity then remains low up to 64.56 m. In this interval, the VGP in the Northern Hemisphere moves into the Southern Hemisphere between depths of 65.69 and 65.67 m, and the VGP moves to cluster D at ~65.17 m. Afterwards, the relative paleointensity gradually increases. From 64.65 to 63.46 m, the VGP settles in cluster E, and then, the VGP moves to the area near the Antarctic.

During the polarity reversal, especially between depths of 67.03 and 63.46 m, the relative paleointensity drops to approximately 12 % of the maximum value. After the large movements in the VGP, the relative paleointensity remains low for a time and then gradually recovers. At 58.38 m depth, the relative paleointensity returns to the peak value observed at 67.75 m, just before the paleomagnetic directional change began, and at about

Kusu *et al. Progress in Earth and Planetary Science* (2016) 3:26

Page 9 of 13

Fig. 7 Paleomagnetic results in the vicinity of the upper Olduvai polarity reversal. Comparison between Core M and ODP Site 983. **a** VGP path. **b** VGP latitude. **c** Relative paleointensity ($NRM_{20-40 \, mT}/ARM_{20-40 \, mT}$) from Core M and Core I. **d** VGP path. **e** VGP latitude. **f** Relative paleointensity ($NRM_{20 \, mT}/ARM_{20 \, mT}$) from ODP Site 983. For Site 983, the VGP positions and age model are based on Channell et al. (2002), and the relative paleointensity is based on Mazaud and Channell (1999). The declination and inclination data from ODP Site 983 are plotted using the PANGEA database (Channell et al. 2013). The *dotted circles* in **a** and **d** and the *shaded circles* in **b** and **e** indicate VGP clusters, and the *bold letters* represent the temporal order. The *blue shaded areas* in **a** indicate that the vertical component of the NAD field at the Earth's surface is less than −15 μT (Constable 2007). The *stars* indicate the core sites

55 m, the relative paleointensity becomes comparable to the maximum value observed pre-reversal.
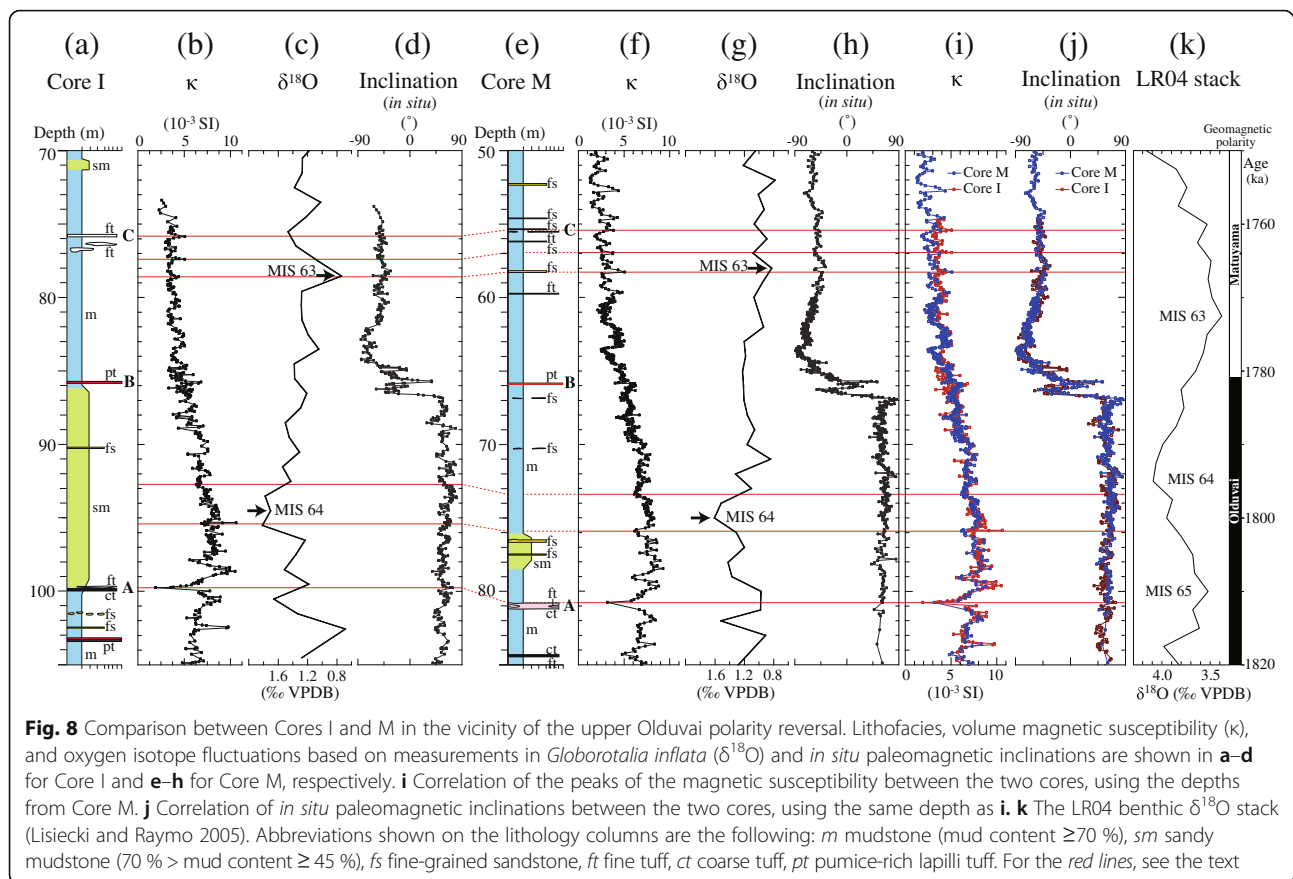
Age model

To construct an age model for the interval spanning the upper Olduvai polarity reversal (1.8–1.7 Ma) in Core M, we correlated our $\delta^{18}O$ profile generated from tests of *G. inflata* in the core (Fig. 8g) with the LR04 global $\delta^{18}O$ stack (Lisiecki and Raymo 2005; Fig. 8k) and determined the peaks of marine isotope stages (MIS) 64 and 63.

The peak observed at 75.00 m (1.61 ‰) is comparable to the peak of MIS 64 because it is just below the Olduvai termination, and the broad low at approximately 58.00–52.00 m (0.78–0.83 ‰) can be correlated to MIS 63 because it is just above the Olduvai termination. The maximum amplitude of $\delta^{18}O$ in the core is 0.83 ‰. This is quite comparable to the amplitude of 0.71 ‰ observed in the LR04 stack between MIS 64 and MIS 63. We therefore assigned the peak at 75.00 m and

the broad low at approximately 58.00–52.00 m to MIS 64 and to MIS 63, respectively.

It is, however, difficult to determine a particular position within the broad trough at approximately 58.00–52.00 m for correlation with the lowest point of MIS 63. To determine which position is suitable as the MIS 63 trough, we used Core I, which was drilled in the same study area (Fig. 1c). From Core I, the Olduvai termination boundary, magnetic susceptibility, and relative paleointensity were obtained, and a significant trough comparable to MIS 63 was recognized in the $\delta^{18}O$ curve (Kusu et al. 2014). The relative paleointensity and $\delta^{18}O$ curve for Core I were determined using the same methods as in this study for Core M. Figure 8 shows a comparison between the two cores and includes the horizons of MISs 64 and 63. The vertical axes are expressed as core depths. Because a coarse-grained tuff bed, a pumice-rich lapilli tuff bed, and a fine-grained tuff bed (A, B, C, respectively, in Fig. 8) are commonly recognized in both cores, these three tephra beds were used

Kusu *et al. Progress in Earth and Planetary Science* (2016) 3:26

Page 10 of 13

Fig. 8 Comparison between Cores I and M in the vicinity of the upper Olduvai polarity reversal. Lithofacies, volume magnetic susceptibility (κ), and oxygen isotope fluctuations based on measurements in *Globorotalia inflata* (δ¹⁸O) and *in situ* paleomagnetic inclinations are shown in **a–d** for Core I and **e–h** for Core M, respectively. **i** Correlation of the peaks of the magnetic susceptibility between the two cores, using the depths from Core M. **j** Correlation of *in situ* paleomagnetic inclinations between the two cores, using the same depth as **i**. **k** The LR04 benthic δ¹⁸O stack (Lisiecki and Raymo 2005). Abbreviations shown on the lithology columns are the following: *m* mudstone (mud content ≥70 %), *sm* sandy mudstone (70 % > mud content ≥ 45 %), *fs* fine-grained sandstone, *ft* fine tuff, *ct* coarse tuff, *pt* pumice-rich lapilli tuff. For the *red lines*, see the text

to correlate the two cores. In the interval between the coarse-grained tuff bed (A) and the fine-grained tuff bed (C), the fluctuating patterns in the two cores' magnetic susceptibility records coincide well (Fig. 8i), as do the records of *in situ* paleomagnetic inclinations (Fig. 8j). We therefore used the magnetic susceptibility curves to more closely correlate the two cores. The red lines in Fig. 8 indicate the correlation between the two cores using representative tie horizons in the vicinities of MIS 64 and MIS 63.

From this correlation, we determined that the most likely position corresponding to the trough of MIS 63 in Core M is at a depth of 58.00 m. We assigned MIS 64 (1795.0 ka) to the peak at 75.00 m and MIS 63 (1772.5 ka) to the trough at 58.00 m, which serves as an age model for Core M. Based on the age model, the average sedimentation rate between MISs 64 and 63 is 73.9 cm/kyr.

Discussion

Our results from Cores M and I show that the fluctuating patterns in the records of magnetic susceptibility (Fig. 8i), *in situ* paleomagnetic inclinations (Fig. 8j), and relative paleointensities (Fig. 7c) coincide well with each other, and the ChRM inclinations of Core M are in close

agreement with the value expected for a geocentric axial dipole (Fig. 6c). This supports the reliability of our results for the upper Olduvai polarity transition.

The VGP latitudes and relative paleointensities are plotted against age in Fig. 7b, c, respectively. If the polarity transition interval is defined as the interval when the VGPs cross the equator and are more than 45° apart from the geographical poles, the transitional interval for Core M lies between depths of 66.99 and 63.60 m. This interval is dated at between 1784.4 and 1779.9 ka, and the duration of the transition is thus estimated to be 4.5 kyr. The relative paleointensity evidently decreased rapidly approximately 1 kyr before the beginning of the polarity transition and gradually recovered to its original value after almost 12 kyr.

The VGP cluster over the southern South Atlantic has a similar location to VGP clusters seen in lava-derived records of polarity transitions spanning the last 10 Myr (Hoffman 1991, 1992). Previous studies suggest that the VGP cluster areas during polarity transitions are associated with the vertical flux patches in the present non-axial dipole (NAD) field, although the VGP records from different polarity transitions merge (e.g., Channell et al. 2003, 2004; Hoffman et al. 2008). In Fig. 7a, the blue-shaded areas indicate the downward flux patches of the

Kusu *et al. Progress in Earth and Planetary Science* (2016) 3:26

Page 11 of 13

NAD, averaged for the last 400 years, where the vertical component is less than –15 μT (Constable 2007). This figure shows that our results of the VGPs from the upper Olduvai polarity transition match well with the NAD vertical flux patches.

The results for the upper Olduvai polarity transition obtained from this study were compared with records from ODP Site 983 (Mazaud and Channell 1999; Channell et al. 2002). At Site 983 (60.40° N, 23.64° W), detailed records of the upper Olduvai polarity transition were obtained by u-channel measurements at 1 cm intervals. Figure 7 compares the VGP path, VGP latitude, and relative paleointensity results of the two studies. The VGP position data and age model from Site 983 are based on Channell et al. (2002), and the relative paleointensity data from this site is based on Mazaud and Channell (1999). Note that the age models used in the two studies are different. The VGP path from the present study does not exhibit the large loop seen in the Site 983 record (Fig. 7d). However, the VGP cluster areas in eastern North America, the South Atlantic, and the Middle East obtained from Site 983 are similar to the areas reported in this study, whereas the VGP paths between the clusters are different. The bold letters in Fig. 7 represent the temporal order of the VGP clusters at each study site. As shown in Fig. 7, the temporal orders of the VGP clusters are different for the two studies, but the positions of the clusters are similar. The two records indicate that the VGP cluster moved to a location close to the study site at the beginning of the transition, relocated to eastern North America, and then relocated to the Southern Hemisphere. This suggests that the VGPs at the beginning of the transition could have been affected by one of the vertical flux patches of the NAD field located near the study site, and that, just before the polarity reversal, the VGPs were strongly affected by the NAD field near eastern North America.

Based on the ten most detailed records of reversals from volcanic materials, Valet et al. (2012) proposed that a geomagnetic reversal can be characterized by three successive phases: a precursor event (phase 1), a 180° polarity switch (phase 2), and a rebound (phase 3). Furthermore, they proposed that the maximum durations of phases 1 and 3 are ~2.5 kyr and the maximum duration of phase 2 is approximately ~1.0 kyr. Our records for VGP cluster A could correspond to phase 1, the VGP path between clusters C and D could correspond to phase 2, and VGP cluster E could correspond to phase 3.

A previous study that analyzed variations in field intensity across the five polarity reversals over the past 2 Myr suggested that the intensity records were characterized by a rapid recovery following the transitions (Valet et al. 2005). However, the relative paleointensity variations during the upper Olduvai polarity transition reconstructed in this study (Fig. 7c) as well as from Site 983 (Fig. 7f) show a slow and gradual recovery after the reversal. Thus, the results from this study and Site 983 suggest that the paleointensity variations associated with geomagnetic reversals could differ between each reversal.

Clement (2004) estimated that the average duration of a polarity transition is approximately 7 kyr, based on data from 30 selected sedimentary records spanning the four most recent polarity reversals (the Matuyama-Brunhes, the upper and the lower Jaramillo, and the upper Olduvai), and that this duration varies with site latitude: shorter durations were observed at low-latitude sites, and longer durations were observed at mid- to high-latitude sites. Our estimated duration of 4.5 kyr for the polarity transition closely matches the durations observed at mid-latitude sites, which range from 3 to 10 kyr, by Clement (2004).

At Site 983, the upper Olduvai polarity transition was recorded between 248 and 247 mcd (Mazaud and Channell 1999). The 248 mcd was dated at 1778 ka using the age model constructed by Channell et al. (2002) based on the astrochronology of Shackleton et al. (1990). For Core M, the upper Olduvai polarity transition was determined to be between depths of 66.99 and 63.60 m. The depth of 66.99 m is dated at 1773.4 ka using an age model also based on the astrochronology of Shackleton et al. (1990). This estimated age from Core M is close to but slightly younger (ca. 4 kyr) than the estimated age from Site 983. The reason for this discrepancy could be partly due to a lock-in depth inherent in the Site 983 sediments. However, we acknowledge that our age model, which consists of only two tie points, has to be improved to allow more precise comparison with other records in terms of reversal timing.

Conclusions

We present a nearly continuous paleomagnetic record of the upper Olduvai polarity reversal from a sediment core (Core M) drilled in southern Yokohama City, on the Pacific side of central Japan. The results of our study are summarized as follows.

(1) In Core M, the reversal boundary was observed between 65.69 and 65.67 m depth (dated to 1782.7 ka), the polarity transition was observed between 66.99 and 63.60 m depth (dated to between 1784.4 and 1779.9 ka), and the duration of the polarity transition is estimated to be 4.5 kyr, based on an age model derived from $\delta^{18}O$ measurements in the planktonic foraminifer *G. inflata* from the same core.

(2) In the polarity transition period, VGP clusters were observed in five areas: eastern Asia near Japan, the Middle East, eastern North America (the North

Kusu *et al. Progress in Earth and Planetary Science* (2016) 3:26

Page 12 of 13

Atlantic), off southern Australasia, and the southern South Atlantic off South Africa. The primary locations of the observed VGP clusters are closely related to the vertical flux patches of the present NAD field.

(3) The relative paleointensity decreased rapidly approximately 1 kyr before the beginning of the polarity reversal and recovered to its original value after almost 12 kyr. Between depths of 67.03 and 63.46 m, where a large movement in the VGPs was observed, the relative paleointensity dropped to approximately 12 % of the maximum value observed pre-reversal.

Additional file

Additional file 1: Table A1. Results from Core M. Natural remanent magnetizations (NRM), characteristic remanent magnetization (ChRM) declinations and inclinations, maximum angular dispersions (MAD), relative paleointensities ($NRM_{20-40\ mT}/ARM_{20-40\ mT}$), volume magnetic susceptibilities (κ), and anhysteretic remanent magnetization susceptibilities (κ_{ARM}). (XLSX 61 kb)

Abbreviations

AFD: Alternating field demagnetization; AMS: Anisotropy of magnetic susceptibility; ARM: Anhysteretic remanent magnetization; ChRM: Characteristic remanent magnetization; MAD: Maximum angular dispersion; MD: Multidomain; MIS: Marine isotope stage; NAD: Non-axial dipole; NRM: Natural remanent magnetization; PSD: Pseudo-single domain; SD: Single domain; THD: Thermal demagnetization; VGP: Virtual geomagnetic pole; κ: Magnetic susceptibility; κ_{ARM}: Anhysteretic remanent magnetization susceptibility

Authors' contributions

MO proposed the paleomagnetic study of polarity transition. CK and MO wrote the manuscript and coordinated the structure of the paper. CK collected the paleomagnetic and rock-magnetic samples, carried out the experiments and measurements, and analyzed the data. AN carried out the geological surveys. RM conducted the drill core research project and contributed to the construction of the manuscript. HW contributed to the isotope analyses. All the authors read and approved the final manuscript.

Competing interests

The authors declare that they have no competing interests.

Author details

[1]Graduate School of Environment and Information Sciences, Yokohama National University, 79-7 Tokiwadai, Hodogaya-ku, Yokohama 240-8501, Japan. [2]College of Science, Ibaraki University, 2-1-1 Bunkyo, Mito, Ibaraki 310-8512, Japan. [3]Hiratsuka City Museum, 12-41 Sengencho, Hiratsuka, Kanagawa 254-0041, Japan. [4]Faculty of Environment and Information Sciences, Yokohama National University, 79-7 Tokiwadai, Hodogaya-ku, Yokohama 240-8501, Japan. [5]Faculty of Science, Shizuoka University, 836 Ohya, Suruga-ku, Shizuoka 422-8529, Japan.

References

Channell JET, Guyodo Y (2004) The Matuyama Chronozone at ODP Site 982 (Rockall Bank): evidence for decimeter-scale magnetization lock-in depths. In: Channell JET, Kent DV, Lowrie W, Meert JG (eds) Timescales of the paleomagnetic field, vol 145, Geophys Monogr Ser. AGU, Washington DC, pp 205–219. doi:10.1029/145GM15

Channell JET, Mazaud A, Sullivan P, Turner S, Raymo ME (2002) Geomagnetic excursions and paleointensities in the Matuyama Chron at Ocean Drilling Program Sites 983 and 984 (Iceland Basin). J Geophys Res 107(B6). doi:10.1029/2001JB000491

Channell JET, Labs J, Raymo ME (2003) The Réunion Subchronozone at ODP Site 981 (Feni Drift, North Atlantic). Earth Planet Sci Lett 215(1):1–12. doi:10.1016/S0012-821X(03)00435-7

Channell JET, Curtis JH, Flower BP (2004) The Matuyama-Brunhes boundary interval (500-900 ka) in North Atlantic drift sediments. Geophys J Int 158(2): 489–505. doi:10.1111/j.1365-246X.2004.02329.x

Channell JET, Xuan C, Hodell DA (2009) Stacking paleointensity and oxygen isotope data for the last 1.5 Myr (PISO-1500). Earth Planet Sci Lett 283(1):14–23. doi:10.1016/j.epsl.2009.03.012

Channell JET, Mazaud A, Sullivan P, Turner S, Raymo ME (2013) Declination and inclination of ODP Site., pp 162–983. doi:10.1594/PANGAEA.808978

Clement BM (1991) Geographical distribution of transitional VGPs: evidence for non-zonal equatorial symmetry during the Matuyama-Brunhes geomagnetic reversal. Earth Planet Sci Lett 104(1):48–58. doi:10.1016/0012-821X(91)90236-B

Clement BM (2004) Dependence of the duration of geomagnetic polarity reversals on site latitude. Nature 428(6983):637–640. doi:10.1038/nature02459

Constable C (2007) Non-dipole field. In: Gubbins D, Herrero-Bervera E (eds) Encyclopedia of geomagnetism and paleomagnetism. Springer, Netherlands, pp 701–704

Day R, Fuller M, Schmidt VA (1977) Hysteresis properties of titanomagnetites: grain size and composition dependence. Phys Earth Planet Int 13(4):260–267. doi:10.1016/0031-9201(77)90108-X

deMenocal PB, Ruddiman WF, Kent DV (1990) Depth of the post-depositional remanence acquisition in deep-sea sediments: a case study of the Brunches-Matuyama reversal and oxygen isotopic stage 19.1. Earth Planet Sci Lett 99:1–13. doi:10.1016/0012-821X(90)90066-7

Dunlop DJ (2002) Theory and application of the Day plot (Mrs/Ms versus Hcr/Hc), 1. Theoretical curves and tests using titanomagnetite data. J. Geophys Res 107(B3). doi:10.1029/2001JB000486

Eto T (1986) Stratigraphy of the Hayama Group in the Miura Peninsula, Japan. Sci Rep Yokohama National Univ (Sec II) 33:67–106

Hoffman KA (1991) Long-lived transitional states of the geomagnetic field and the two dynamo families. Nature 354(6351):273–277

Hoffman KA (1992) Dipolar reversal states of the geomagnetic field and core-mantle dynamics. Nature 359(6398):789–794

Hoffman KA, Singer BS, Camps P, Hansen LN, Johnson KA, Clipperton S, Carvallo C (2008) Stability of mantle control over dynamo flux since the mid-Cenozoic. Phys Earth Planet Int 169(1):20–27. doi:10.1016/j.pepi.2008.07.012

Hyodo M (1984) Possibility of reconstruction of the past geomagnetic field from homogeneous sediments. J Geomag Geoelectr 36:45–62. doi:10.5636/jgg.36.45

Irving E, Major A (1964) Post-depositional detrital remanent magnetization in a synthetic sediment. Sedimentology 3(2):135–143. doi:10.1111/j.1365-3091.1964.tb00638.x

Kent DV (1973) Post-depositional remanent magnetisation in deep-sea sediment. Nature 246(5427):32–34

King JW, Banerjee SK, Marvin J (1983) A new rock-magnetic approach to selecting sediments for geomagnetic paleointensity studies: application to paleointensity for the last 4000 years. J Geophys Res 88:5911–5921

Kusu *et al. Progress in Earth and Planetary Science* (2016) 3:26

Page 13 of 13

Kirschvink JL (1980) The least-squares line and plane and the analysis of palaeomagnetic data. Geophys J Int 62:699–718. doi:10.1111/j.1365-246X.1980.tb02601.x

Kitazaki T, Majima R (2003) A slope to outer-shelf cold-seep assemblage in the Plio-Pleistocene Kazusa Group, Pacific side of central Japan. Paleontol Res 7:279–296

Kusu C, Nozaki A, Okada M, Wada H, Majima R (2014) Lithology and upper boundary of the Olduvai Subchronozone in a core recovered from the middle Kazusa Group (Lower Pleistocene) on the Miura Peninsula, Pacific side of central Japan. J Geol Soc Jpn 120:53–70. doi:10.5575/geosoc.2014.0002

Laj C, Mazaud A, Weeks R, Fuller M, Herrero-Bervera E (1991) Geomagnetic reversal paths. Nature 351:477. doi:10.1038/351447a0

Lisiecki LE, Raymo ME (2005) A Pliocene-Pleistocene stack of 57 globally distributed benthic $\delta^{18}O$ records. Paleoceanography 20:PA1003. doi:10.1029/2004PA001071

Mazaud A, Channell JET (1999) The top Olduvai polarity transition at ODP Site 983 (Iceland Basin). Earth Planet Sci Lett 166:1–13. doi:10.1029/2001JB000491

Mazaud A, Channell JET, Xuan C, Stoner JS (2009) Upper and lower Jaramillo polarity transitions recorded in IODP Expedition 303 North Atlantic sediments: implications for transitional field geometry. Phys Earth Planet Int 172(3):131–140. doi:10.1016/j.pepi.2008.08.012

Merrill RT, McFadden PL (1999) Geomagnetic polarity transitions. Rev Geophys 37(2):201–226

Mitsunashi T, Suda Y (1980) Geological map of Japan 1: 200 000, Otaki. Geol Surv Japan, Tsukuba

Mitsunashi T, Ono K, Suda Y (1980) Geological map of Japan 1:200 000, Yokosuka. Geol Surv Japan, Tsukuba

Nozaki A, Majima R, Kameo K, Sakai S, Kouda A, Kawagata S, Wada H, Kitazato H (2014) Geology and age model of the Lower Pleistocene Nojima, Ofuna, and Koshiba Formations of the middle Kazusa Group, a forearc basin-fill sequence on the Miura Peninsula, the Pacific side of central Japan. Island Arc 23:157–179. doi:10.1111/iar.12066

Oba T, Irino T, Yamamoto M, Murayama M, Takamura A, Aoki K (2006) Paleoceanographic change off central Japan since the last 144 000 years based on high-resolution oxygen and carbon isotope records. Glob Planet Change 53:5–20

Ohno M, Murakami F, Komatsu F, Guyodo Y, Acton G, Kanamatsu T, Evans HF, Nanayama F (2008) Paleomagnetic directions of the Gauss-Matuyama polarity transition recorded in drift sediments (IODP Site U1314) in the North Atlantic. Earth Planets Space 60:e13–e16

Okada M, Niitsuma N (1989) Detailed paleomagnetic records during the Brunhes-Matuyama geomagnetic reversal, and a direct determination of depth lag for magnetization in marine sediments. Phys Earth Planet Int 56:133–150

Passier HF, De Lange GJ, Dekkers MJ (2001) Magnetic properties and geochemistry of the active oxidation front and the youngest sapropel in the eastern Mediterranean Sea. Geophys J Int 145(3):604–614

Sakamoto T, Sakai A, Hata M, Unozawa A, Oka S, Hiroshima T, Komazawa M, Murata Y (1987) Geological Map of Japan 1: 200 000, Tokyo. Geol Surv Japan, Tsukuba

Seno T, Takano T (1989) Seismotectonics at the trench-trench-trench triple junction off central Honshu. Pure Appl Geophys 129:27–40

Shackleton NJ, Berger A, Peltier WR (1990) An alternative astronomical calibration of the lower Pleistocene timescale based on ODP Site 677. Trans R Soc Edinburgh Earth Sci 81:251–261

Suganuma Y, Yokoyama Y, Yamazaki T, Kawamura K, Horng CS, Matsuzaki H (2010) ^{10}Be evidence for delayed acquisition of remanent magnetization in marine sediments: implication for a new age for the Matuyama-Brunhes boundary. Earth Planet Sci Lett 296(3):443–450. doi:10.1016/j.epsl.2010.05.031

Suganuma Y, Okuno J, Heslop D, Roberts AP, Yamazaki T, Yokoyama Y (2011) Post-depositional remanent magnetization lock-in for marine sediments deduced from ^{10}Be and paleomagnetic records through the Matuyama-Brunhes boundary. Earth Planet Sci Lett 311(1):39–52. doi:10.1016/j.epsl.2011.08.038

Takahashi N, Mitsuoka T, Katoh A, Yokoyama K (2005) Correlation of the key tephra bed 'Kd38' occurring near the boundary between the Tertiary and Quaternary in the southern part of the Kanto Province, central Japan: correlation in the Kazusa Group and the Chikura Group, Boso Peninsula. J Geol Soc Jpn 111:371–388

Tate Y, Majima R (1998) A chemosynthetic fossil community related to cold seeps in the outer shelf environment: a case study in the Lower Pleistocene Koshiba Formation, Kazusa Group, central Japan. J Geol Soc Jpn 104:24–41

Tauxe L (1993) Sedimentary records of relative paleointensity of the geomagnetic field: theory and practice. Rev Geophys 31:319–354

Tauxe L, Yamazaki T (2007) Paleointensities. In: Schubert G (ed) Treatise on geophysics, vol 5, 1st edn. Elsevier, Amsterdam, pp 509–563

Tauxe L, Herbert T, Shackleton NJ, Kok YS (1996) Astronomical calibration of the Matuyama–Brunhes boundary: consequences for magnetic remanence acquisition in marine carbonates and the Asian loess sequences. Earth Planet Sci Lett 140:133–146. doi:10.1016/0012-821X(96)00030-1

Tauxe L, Steindor JL, Harris A (2006) Depositional remanent magnetization: toward an improved theoretical and experimental foundation. Earth Planet Sci Lett 244:515–529. doi:10.1016/j.epsl.2006.02.003

Tric E, Laj C, Jéhanno C, Valet JP, Kissel C, Mazaud A, Iaccarino S (1991) High-resolution record of the Upper Olduvai transition from Po Valley (Italy) sediments: support for dipolar transition geometry? Phys Earth Planet Int 65(3):319–336

Unozawa A, Oka S, Sakamoto T, Komazawa M (1983) Geological map of Japan 1: 200 000, Chiba. Geol Surv Japan, Tsukuba

Utsunomiya M, Majima R (2012) Paleobathymetries of the Plio-Pleistocene Urago and Nojima Formations, Kazusa Group, Miura Peninsula, central Japan: revision on the basis of molluscan fossils from new localities. Fossils (Palaeontological Soci Jpn) 91:5–14

Valet JP, Meynadier L, Guyodo Y (2005) Geomagnetic dipole strength and reversal rate over the past two million years. Nature 435(7043):802–805

Valet JP, Fournier A, Courtillot V, Herrero-Bervera E (2012) Dynamical similarity of geomagnetic field reversals. Nature 490(11491):89–93. doi:10.1038/nature11491

Verosub KL (1977) Depositional and postdepositional processes in the magnetization of sediments. Rev Geophys 15(2):129–143

Wada H, Fujii N, Niitsuma N (1984) Analytical method of stable isotope for ultra-small amounts of carbon dioxide with MAT250 mass-spectrometer. Geosci Repts Shizuoka Univ 10:103–112

Yamazaki T, Oda H (2005) A geomagnetic paleointensity stack between 0.8 and 3.0 Ma from equatorial Pacific sediment cores. Geochem Geophys Geosys 6(11):Q11H20. doi:10.1029/2005GC001001

Zijderveld JDA (1967) A. C. demagnetization of rocks: analysis of results. In: Collinson DW, Creer KM, Runcorn SK (eds) Methods in palaeomagnetism. Elsevier, Amsterdam, pp 254–286